International Journal of Nanomedicine

Dovepress
Taylor & Francis Group

Open Access Full Text Article

ORIGINAL RESEARCH

Melanin Nanoparticles as a Safe and Effective Iron Chelation Therapy: An ex vivo Assessment of Human Placental Transfer in Pregnant Beta-Thalassemia

Nahla Bakhamis[1], Toluwalase Awoyemi[1], Manu Vatish[1], Helen Townley[1,2]

[1]Nuffield Department of Women's & Reproductive Health, University of Oxford, Oxford, UK; [2]Department of Engineering Science, University of Oxford, Oxford, UK

Correspondence: Helen Townley, Oxford University, Begbroke Science Park, Woodstock Road, Oxford, OX5 1PF, United Kingdom, Tel +44 1865 283792, Email helen.townley@wrh.ox.ac.uk

Background: Iron toxicity is a major contributor to adverse pregnancy outcomes in women with transfusion-dependent thalassemia. Currently used iron chelators are not recommended during pregnancy, as they can cross the placenta causing potential risk to the fetus. However, ceasing medication may adversely affect the mother's health in both the short- and long-term.

Objective: We previously demonstrated that melanin nanoparticles can effectively chelate iron, and this has been confirmed by others in iron-overloaded mice. This study aims to assess whether these nanoparticles cross the placenta and evaluate their biocompatibility and haemocompatibility.

Study Design: A library of 50 nm, 200 nm, and 500 nm melanin nanoparticles were synthesized and coated with Polyethylene Glycol (PEG) to improve their stability. The particles were tested for chelating iron efficacy in and biocompatibility. An in vitro BeWo (choriocarcinoma) cell model and ex vivo human placental perfusion system were used to assess nanoparticle transplacental passage.

Results: Melanin nanoparticles of all sizes were able to chelate iron with a maximum adsorption of 14 mm iron/g of material; significantly higher than Desferrioxamine (DFO) of the same concentration. It was also determined that PEGylated melanin nanoparticles with appropriate size (cut off 200 nm) could be restricted from passing across the placental barrier in an in vitro model using a human choriocarcinoma cell line and in an ex vivo human placental perfusion model. The particles did not cause red cell haemolysis or blood clotting at concentrations up to 1 mM.

Conclusion: It was demonstrated herein that transport of MNPs across the placental barrier is highly dependent on particle size (cut off size of 200 nm PEGylated MNPs). Findings suggest the possibility of providing a safe method of iron chelation during pregnancy. Future work using in vivo models will be applied to study systemic particle interactions.

Plain Language Summary: At present, clinicians are faced with the choice of whether to continue maternal chelation therapy with possible risk to the fetus, or to cease medication with risk to the mother. The latter may adversely affect the mother's health long after delivery of the baby. Although there are very few clinical trials on using DFO during pregnancy, the use of the small MW DFO on pregnant women is contraindicated. Thus, DFO is classified by the Food and Drug Association as category C during pregnancy due to severe skeletal anomalies and teratogenic effects reported in animal studies. PEGylated melanin nanoparticles (MNPs) of 200 nm or larger are unable to cross the placenta, as shown in both an in vitro BeWo cell model and an ex vivo human placental perfusion model. These findings suggest that MNPs may be a safer option for iron chelation during pregnancy. However, pre-clinical animal testing and clinical trials are needed to determine overall interactions of MNPs in *vivo* before routine use in a clinical setting.

The exclusion of pregnant women from clinical trials has limited research on medications specifically designed for pregnancy with only a couple of drugs developed in the past four decades.[1] There is a critical need to fill the knowledge gap regarding safer and effective therapeutics in this population. The use of clinically approved nanoparticles in pregnancy has increased rapidly; with the Covid 19 vaccines developed by Pfizer and Moderna being prominent examples. These vaccines have been used in a large population of pregnant women without reports of unfavorable complications,[2] paving the way for more nanoparticle medications to be used in the future.

Received: 12 October 2024
Accepted: 30 January 2025
Published: 18 April 2025

Graphical Abstract

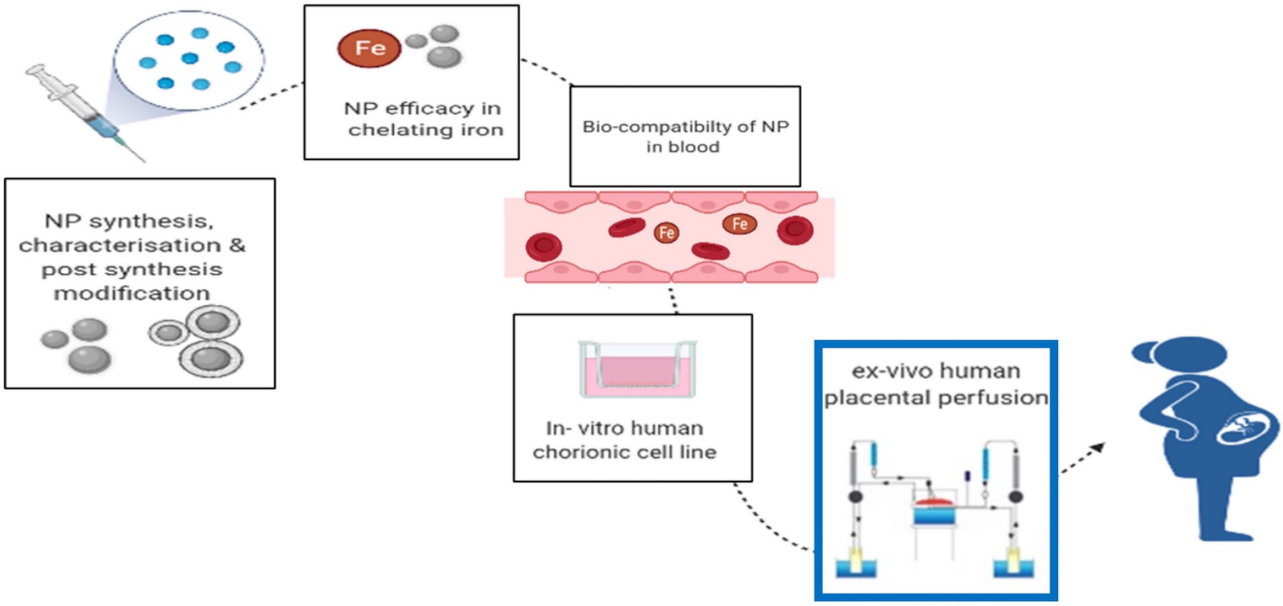

Keywords: Melanin, nanoparticles, beta thalassemia, placenta, iron chelation, BeWo, PEGylation

Introduction

The life expectancy of most patients with beta thalassemia major (β-TM) has markedly improved; largely due to the management of iron overload secondary to frequent blood transfusions. As a result, most women with β-TM survive beyond puberty. While iron overload can affect fertility through damage to the anterior pituitary, many women can still achieve pregnancy, either spontaneously or with gonadotrophins.[3,4] β-TM pregnancies, however, are at high risk due to the complications of iron overload [5–7] including hepatic, cardiac, and endocrine dysfunction, with concerns around cardiomyopathy and increased risk of fetal growth restriction. Pregnant women with β-TM require close monitoring of iron status and a multidisciplinary team approach from pre-conception to post-partum to ensure optimal outcomes.[4,5,8]

Although iron overload may threaten the mother's life even long after delivery, iron chelation therapy is mostly withheld during pregnancy, as currently used chelators [desferrioxamine (DFO), deferiprone (DFP), and deferasirox (DFX)], may cross the placenta causing potential risk to the fetus.[4,7] Withholding treatment puts the mother at increased risk of new onset endocrine disorders such as diabetes mellitus, hypothyroidism, and hypoparathyroidism.[9] However, fetal mice and rabbits exposed to DFO and DFX have shown teratogenic effects, delayed ossification, and skeletal anomalies.[4]

A chelation agent is needed for use during pregnancy that does not cross the placental barrier. One potential solution is a nanoparticle iron chelator. The interaction between nanoparticles and cells/tissues is determined by particle characteristics and functionalization; factors which can be readily manipulated at the synthesis stage (Supplementary Figure 1).[10,11] Previous studies using silica, gold, polystyrene, and liposome nanoparticles have shown that the interaction of nanoparticles with mice and human placenta is mainly affected by particle size (Table 1). Thus, it is likely that a nanoparticulate chelator of an appropriate size could be restricted from movement across the placenta, and safely used to treat the mother.

Melanin is known to naturally chelate iron to protect cells from the Fenton reaction and oxidative stress. Synthetic melanin nanoparticles (MNPs) can mimic the physical and chemical properties of natural melanin in the body, including

Table 1 The Effect of Nanoparticles Size in Crossing the Placenta

NP Type	Size	Crossed Placenta	Experimental Model
Silica	70 nm	Yes	Mice[14]
	300 nm	No	Mice[14]
	1000 nm	No	Mice[14]
	25 and 50 nm Rhodamine labelled	Yes	Ex vivo human placenta[15]
Gold	1.5 nm	Yes	Rat[16]
	18 nm	No	Rat[16]
	80 nm	No	Rat[16]
	3 nm PEG	Yes	Ex vivo human placenta[17]
	10 nm PEG	No	Ex vivo human placenta[18]
	30 nm PEG	No	Ex vivo human placenta[18]
Liposomes	75–100 nm	Yes	Mice[19]
	200 nm	No	Ex vivo human placenta[20]
Polystyrene	20–500 nm	Yes	Mice[21]
	50–240 nm	Yes	Ex vivo human placenta[22]
	500 nm	No	Ex vivo human placenta[22]

Abbreviations: NP, nanoparticle; PEG, PEGylated particles.

the ability to chelate iron.[12] Previous studies in iron-overloaded mice have shown that MNPs can effectively chelate iron more efficiently, with a favourable safety profile and longer circulation half-life compared to DFO.[13]

The aim of this study was to establish a library of melanin nanoparticles of different sizes and to determine their biocompatibility, haematocompatibility, and passage or restriction across the placental barrier. This was achieved by a combination of in *vitro* transwell models of choriocarcinomic cell lines and ex *vivo* human placental perfusion.

Materials and Methods

All chemicals were from Sigma-Aldrich (Gillingham, UK), unless otherwise listed, no financial or other support was received from Sigma-Aldrich for this study.

Patient Samples

Before donation, women were given a participant information sheet concerning the nature of the research and provided written informed consent if they agreed to donate their placentae. Samples were collected from women at the John Radcliffe Hospital (Oxford, UK). This study was conducted in accordance with the principles of the Declaration of Helsinki and was approved by the Oxford Research Ethics Committee C (REC ref no. 07/H0606/148 and 07/H0607/74).

Cell Lines and Cell Culture

BeWo b30 (Caltag Medsystems; Cat. # C003002) and HepG2 (a gift from Dr. Ricky Bogal, University of Birmingham) were used for experiments. The use of these cells was approved by the Oxford Research Ethics Committee C (REC ref no. 07/H0606/148 and 07/H0607/74). All cells were expanded, and frozen stocks were made within a few passages of receipt. Early passages were then thawed and used for this study. The cell line used in this study was carefully authenticated through morphological examination which provides strong evidence supporting the authenticity of the cell line used. BeWo cells were cultured in complete Dulbecco's Modified Eagles Medium – high glucose (DMEM) and F12-K media, and HepG2 cells were cultured in RPMI media. All media was supplemented with 10% (v/v) Fetal Bovine Serum (FBS), 2 mM L-glutamine, 100 U/mL penicillin, and 0.1 mg/mL streptomycin. Both cell lines were incubated at

37 °C/ 5% CO_2 and passaged when confluent. In some experiments, cells were treated with 50 μM forskolin (Sigma Aldrich, Gillingham, UK) to induce differentiation.

Melanin Nanoparticle Synthesis

MNPs were produced by hydroxylation of dopamine hydrochloride followed by polymerization. In brief, dopamine hydrochloride (180 mg) was dissolved in 90 mL ddH_2O during the synthesis of 200 nm and 50 nm MNPs, or in 45 mL ddH2O for the synthesis of 500 nm MNPs. The mixture was first heated to 50°C. Subsequently, 950 μL, 760 μL, or 670 μL of 1M NaOH was added to the mixture for 50, 200 and 500 nm MNPs, respectively. The solution was stirred vigorously at 50°C and aged for five hours. Particles were then retrieved by centrifugation at 12,000 rpm for 20 minutes and washed twice with ddH2O. Centrifugation was repeated at 4,000 rpm for 10 minutes to remove any large materials.

MNPs were PEGylated following the method described in Zhang et al.[23] Briefly, the particles were incubated with mPEG-5000 at pH 10 for 12 hours at room temperature with vigorous stirring. Unreacted mPEG was removed by washing three times with ddH_2O. The particles were then freeze-dried overnight, and PEGylation confirmed by infra-red (IR) analysis (Varian Excalibur). An IR absorption reference control spectrum was obtained at 25°C using 4 cm^{-1} resolution using synthetic dried melanin (MP Biomedicals, UK).

An aliquot of the particles was labelled with Rhodamine B to track their movement across the placenta. In situ fluorophore modification of MNPs and MNP-PEG was adapted from Amin et al[24] by including 50 μg mL^{-1} Rhodamine B during synthesis, followed by washing with ddH_2O to remove any unbound Rhodamine.

Physical Characterization

The hydrodynamic diameter of the particles was measured using a Disc centrifuge (DC 24000; CPS Instruments Europe) operated at 24,000 rpm. A density gradient of 8% (w/v) and 24% (w/v) sucrose solution was built with increasing concentrations followed by injection of 100 μL MNP or MNP-PEG suspension for size measurement. All particles were measured against a calibration standard of known size (0.46 μm PVC; CPS Instruments, Europe).

Zeta potential was measured with a Zetasizer (Malvern Nano ZS instrument) by injecting MNPs, and MNP-PEG diluted in ddH_2O into a disposable folded capillary cell (Malvern, Worcestershire, UK).

Particles were imaged by transmission electron microscopy (TEM; JEOL-2100, JEOL-Japan), and scanning electron microscopy (SEM; Carl Zeiss Evo LS15 VP-SEM). Before imaging with primary energy of 15 kV, SEM particles were dry-cast overnight onto a carbon adhesive disc then sputter-coated with 3 nm Au-Pd. Gatan 3 was used for image analysis and size distribution was calculated by measuring at least 50 particles/field.

Efficacy of Iron Chelation

A colorimetric assay was used to assess iron binding to MNPs.[25] Briefly, a final concentration of 1 mM MNP, MNP-PEG, or DFO was incubated with 1, 3, or 4 mM $FeSO_4$ for 24 or 48 hrs at 37°C, before collection by centrifugation at 15,000 rpm for 3 minutes. The supernatant containing unbound iron was collected and further incubated with 1/10 volume sodium acetate buffer (equal volumes of 6M acetic acid and 5M NaOH) for 10 min at RT.

Hydroxylamine (10 μL) was then added and incubated for 10 minutes followed by addition of 100 μL of 0.1 wt % phenanthroline for the colour reaction to take place. Absorbance was measured at 450 nm against a standard calibration curve of $FeSO_4$ ($R^2 = 0.99$).

MNPs ability to chelate the intracellular labile iron pool in HepG2 cells was assessed using a calcein assay and flow-cytometry. HepG2 cells were first seeded in a 12 well plate and treated with 2% (v/v) FBS and holo-transferrin, or with 200 μM iron from ferric ammonium citrate, for 24 hours. Cells were then treated with an equal concentration of DFO, MNP, MNP-PEG or phosphate buffered saline (PBS) for 1 hour. After washing the cells twice with PBS, a 1 mL cell suspension ($0.1–5.0\times10^6$ cells/mL) was incubated with 2 μL of 50 μM calcein AM (Cambridge Bioscience Ltd, UK) for 15–20 minutes at 37°C. Cells were then washed twice and analysed by flow-cytometry for a minimum of 10,000 events. Data were analysed using FlowJo v.10 (BD Biosciences, UK).

The amount of iron in HepG2 cells was determined by employing Calcein as a fluorescent probe for the labile iron pool in the cell lysate and reported as iron/ mg of protein. The latter was determined by Bradford assay of the cell lysate.

Blood Interaction

Haemolysis was measured by suspending red blood cells (RBCs) in PBS (1/10) and incubating with an equal amount of either (i) Triton X-100, (ii) PBS, (iii) 250 μM MNP, (iv) 1mM MNP, (v) 250 μM MNP-PEG, or (vi) 1mM MNP-PEG, for 1 hour at 37°C. The samples were then centrifuged to pellet, and the supernatant was transferred to a 96 well plate to measure the absorption of the released haemoglobin at 595 nm. The haemolysis ratio (HR) then calculated as [HR (%) = (OD test – OD negative control)/ (OD positive control – OD negative control)].

Clotting time was measured by incubating 1 mL citrated blood with Polyethylenimine (PEI), PBS, MNP, or MNP-PEG for 5 minutes at 37°C in glass tubes, followed by the addition of 500 μL of a 25 mm calcium chloride solution. All the tubes were then placed in a water bath (37°C) and inclined up to 180° every 15 seconds, and clotting time was recorded when the blood stopped flowing in the tube.

Transwell Model with BeWo Cell Lines

BeWo cells were seeded in the apical chamber of a 3.0 μm pore polycarbonate insert transwell plate (Scientific Laboratory Supplies Limited) at a seeding density of 1×10^5 cells/cm^2 in 0.5 mL phenol-red-free media plus 50 μM Forskolin to induce fusion. The basal chamber contained 1.5 mL phenol-red-free media. The entire assembly was incubated at 37°C and 5% CO_2 to achieve equilibrium (Supplementary Figure 2A). After 24 hours, 10 μM FITC- dextran (40 kDa) was added to the apical chamber and incubated for 30 minutes at 37°C. Media (50 μL) was then collected from the basal chamber and placed in triplicate in a 96 well plate. The fluorescence was measured at Ex. 465 nm/ Em. 510 nm. The procedure was repeated until the fluorescence was negligible. On day 4 post- seeding the membranes were cut and placed on a glass slide, fixed with 4% (v/v) paraformaldehyde, and stained with 1/100 dilution of either mouse anti-E-cadherin or rabbit anti-zona occludens-1 (ZO-1; Insight Biotechnology Ltd) for 1 hour. Either secondary goat anti-mouse IgG Alexa Fluor 488 conjugate or Alexa Fluor 568 donkey anti-rabbit IgG antibody (BioLegend) were added at a dilution of 1/250 for 1 hour at room temperature, and then mounted with VECTASHIELD media containing DAPI (Supplementary Figure 2B). Confocal images were acquired using confocal microscopy UltraView spinning disk system (PerkinElmer) comprising CSU-X1 spinning disk head (Yokogawa) and Volocity software.

Assessment of the passage of nanoparticles across the membrane was carried out on day 4 post-seeding, and either (i) 100 μM, 250 μM, or 1 mM MNP, or (ii) 100 μM, 250 μM, or 1 mM MNP-PEG, or (iii) 100 μM antipyrine, or (iv) 5 μM FITC-dextran, was added to 0.5 mL phenol red-free media in the apical chamber, and incubated at 37°C and 5% CO_2 (Supplementary Figure 2C). At each time point 100 μL from the basal chamber (and replaced with fresh media) was transferred to a 96 well plate and absorbance was measured at 540 nm to detect MNP/MNP-PEG. Antipyrine was detected using LC (C-18 column), wavelength ranges from 232 to 252 nm. The mobile phase consisted of 60% (v/v) Acetonitrile and 40% (v/v) water.

The cumulative mass transport (ΔQn) was calculated for each time point and corrected for the mass removed from the previous samples as:

$$\Delta Qn = Cn.Vb + \sum_{j=1}^{n-1} Vs.Cj$$

where Cn is the concentration of nanoparticles measured at tn, Vb is the volume in the basal chamber, Vs is the sampling volume, and the summation term represents the correction of the cumulative mass removed by sampling during the sampling period from tn to tn^{-1}. The data was then represented as the basolateral amount of the initial dose (ID) in %.

Ex vivo Human Placental Perfusion

An ex vivo dual lobe placental perfusion system was used as first described by Eaton and Oakey, 1994.[26] Placentae were obtained after informed consent from normal term pregnancies after caesarean section delivery at the John Radcliffe Hospital (Oxford, UK) and processed immediately. After cannulation of the artery and vein of an intact cotyledon, the fetal circulation was inducted at a rate of 5 mL/minute. The placenta was then inverted and laid inside a perspex water jacket maintained at 37°C, followed by perfusion of the maternal side of the identified lobe through six 1.7 mm inside

diameter fetal feeding tubes at a rate of 20 mL/minute. Both maternal (M199 phenol red free + 5 g BSA (1% w/v) + 5000 U/L sodium Heparin + 10 mL antibiotic/antimycotic agent pH 7.4) and fetal (similar to maternal media + 0.8% (w/v) Dextran 20) perfusion media were kept in a water bath at 37 °C, and the maternal media was oxygenated with 95% O_2 and 5% CO_2. The experiment included 30 minutes open perfusion to calibrate the perfusion system and wash the RBCs, then the circuit was closed by ensuring the maternal perfusate flowed back to the maternal media bottle and either 200 nm MNPs or polystyrene NPs were added to the maternal media (Figure 1). Antipyrine (added to the maternal side) was used as a positive control to assess the permeability of the barrier. The experiment was continued for six hours with equal starting volumes (600 mL) of full media on both fetal and maternal sides. Maternal and fetal perfusate (1 mL) were collected prior to the addition of nanoparticles and every hour thereafter; volume loss was calculated for each time point. The pH of the perfusate and the flow rate were continuously monitored to ensure functional integrity of the placenta lobule. Perfusate was centrifuged twice at 1500 g for 10 minutes at 4°C, followed by centrifugation at 10,000 g for 20 minutes to collect the particles. The antipyrine concentration was determined using LC as described above. The

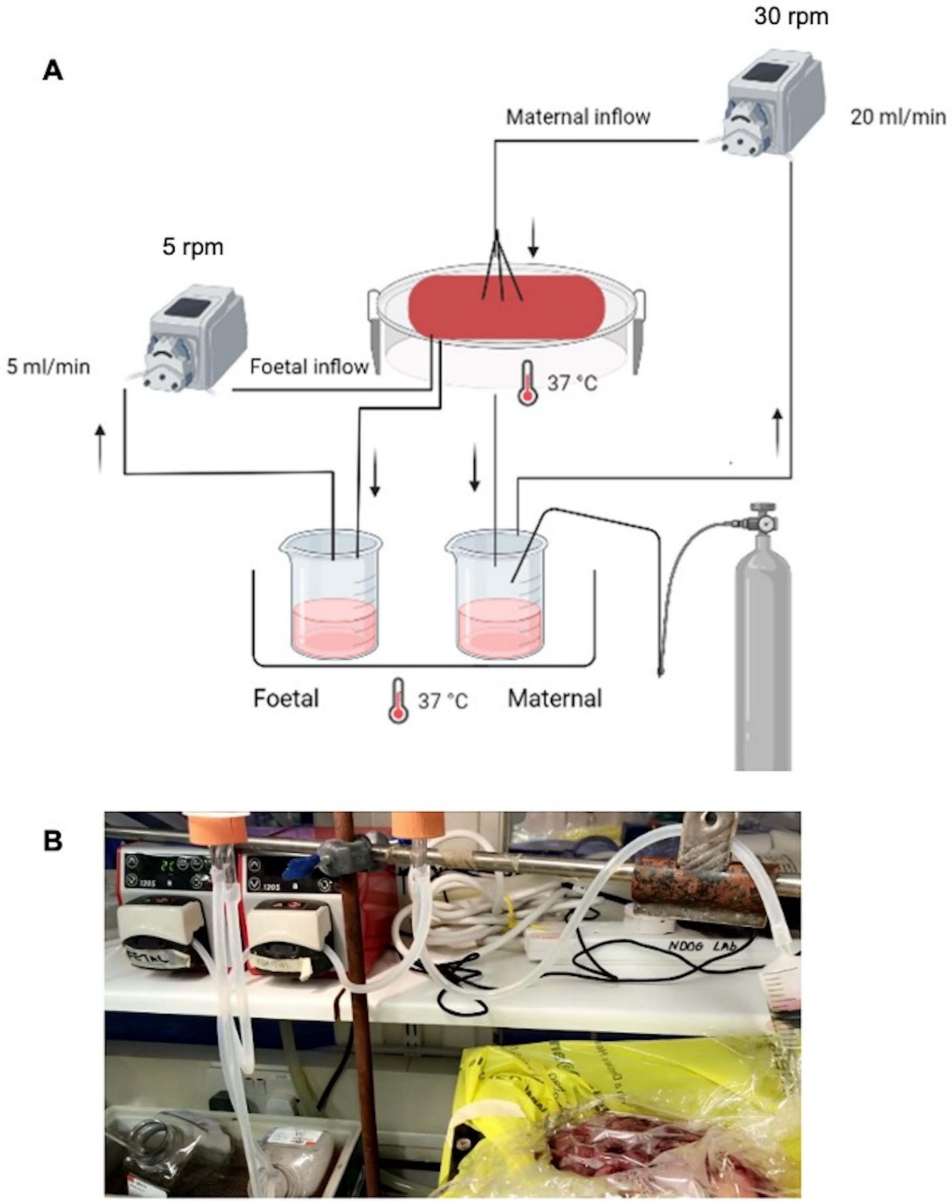

Figure 1 Illustration of the placental perfusion system: (**A**) Diagram showing dual loop placental perfusion system. Image created by Biorender.com (**B**) Image represents a performed placental perfusion on one of the collected samples, rpm; round per minute.

concentration of nanoparticles in the maternal and fetal samples was determined by fluorescent quantification at Ex. 488 nm/ Em. 525 nm, against a standard calibration curve after correction of volume loss. A second assessment was also made using a Zetasizer for particle size.

The criteria for successful perfusion included: volume loss of < 3 mL/hour, antipyrine equilibrium between maternal and fetal side within 3 hours and a fetal pH 7.2 to 7.4 at all times.

Maintenance of the placental function was assessed by measuring the hormonal production of hCG from placental tissue of the perfused lobe by ELISA. hCG ratio was calculated as described in Wick et al (2010):[22] hCG = [(concentration after perfusion – concentration before perfusion) ÷ concentration before perfusion] x 100.

Statistical Analysis

GraphPad Prism 8.0.2 was used for all statistical analysis. Data were compared using One-way Anova or *t*-test. Data are presented as mean ± SD, statistical significance was defined as $P < 0.05$.

Results

Melanin Nanoparticles

The sizes of MNPs as measured by CPS disc centrifuge, peaked at diameters of 60, 250 and 650 nm. TEM and SEM images confirmed the synthesis of MNPs with three different diameters; 50 nm (Figure 2A and B), 200 nm (Figure 2C and D), or 500 nm (Figure 2E) that appeared roughly spherical with a smooth surface. The size distribution was calculated as 50.12 ± 6.15 nm, 194.11 ± 9.51 nm, and 504 ± 10.91 nm by measuring at least 50 particles per field (Figure 2H–J). MNPs showed a good stability with zeta potential ranging from −26 to −32 mV (Figure 2F). Particles were PEGylated to improve their systemic circulation and reduce immunogenicity. PEGylation was confirmed by IR where MNP-PEG showed a peak representing both MNP and PEG (Figure 2G).

Efficacy in Chelating Iron

MNPs of all sizes were able to chelate iron with a maximum adsorption of 14 ± 0.25 mM of iron/g of material; significantly higher than DFO at the same concentration (Figure 3A). There was no significant increase in the amount of adsorbed iron when particles were incubated for longer (Figure 3B), suggesting that particles had reached their saturation capacity. Surface modification with PEG did not significantly limit the ability of MNPs to adsorb iron (Figure 3C).

MNP and MNP-PEG were also able to chelate the labile iron pool in human liver cell lines (HepG2) after loading with iron. Iron overloading in HepG2 cells was achieved by progressive increase of iron, and was assessed using calcein AM staining detected by flow cytometry. Reduced fluorescence intensity of iron loaded cells compared to cells that were not treated with iron is shown (Figure 4A), indicating successful iron overloading in HepG2. The fluorescence intensity of calcein AM was reversed after treatment with DFO (Figure 4B) or 50, 200, or 500 nm MNPs (Figure 4C–E) indicating iron binding to the chelators. MNPs adsorbed significantly higher amounts of iron than DFO at the same concentration (Figure 4G).

Haemocompatibility

No significant difference in clotting time was shown with the largest particles, or with the coated particles compared to controls suggesting a good compatibility. Regarding the 50 nm particles, even though clotting time was significantly shorter compared to a blank control or PBS, it was within the normal clotting time in a glass tube i.e. 6 minutes. Surface modification with PEG showed no significant differences in clotting time compared to non- PEGylated MNPs of all sizes (Figure 5A and B).

Moreover, MNPs and MNP-PEG of all sizes showed less than 5% RBC haemolysis at a concentration of 250 µM. Although this ratio was increased at higher concentrations (1 mM), only the smallest particles almost reached 10% haemolysis (generally compatible),[27] and this was decreased to around 5% (compatible) after surface functionalization with PEG (Figure 5C and D).

Transwell Model with BeWo Cell Lines

To assess the integrity of the BeWo cell barrier layer within the transwell set-up transport of the large molecule FITC-Dextran (40 kDa) was monitored. The concentration of FITC-dextran in the basal chamber gradually decreased until it

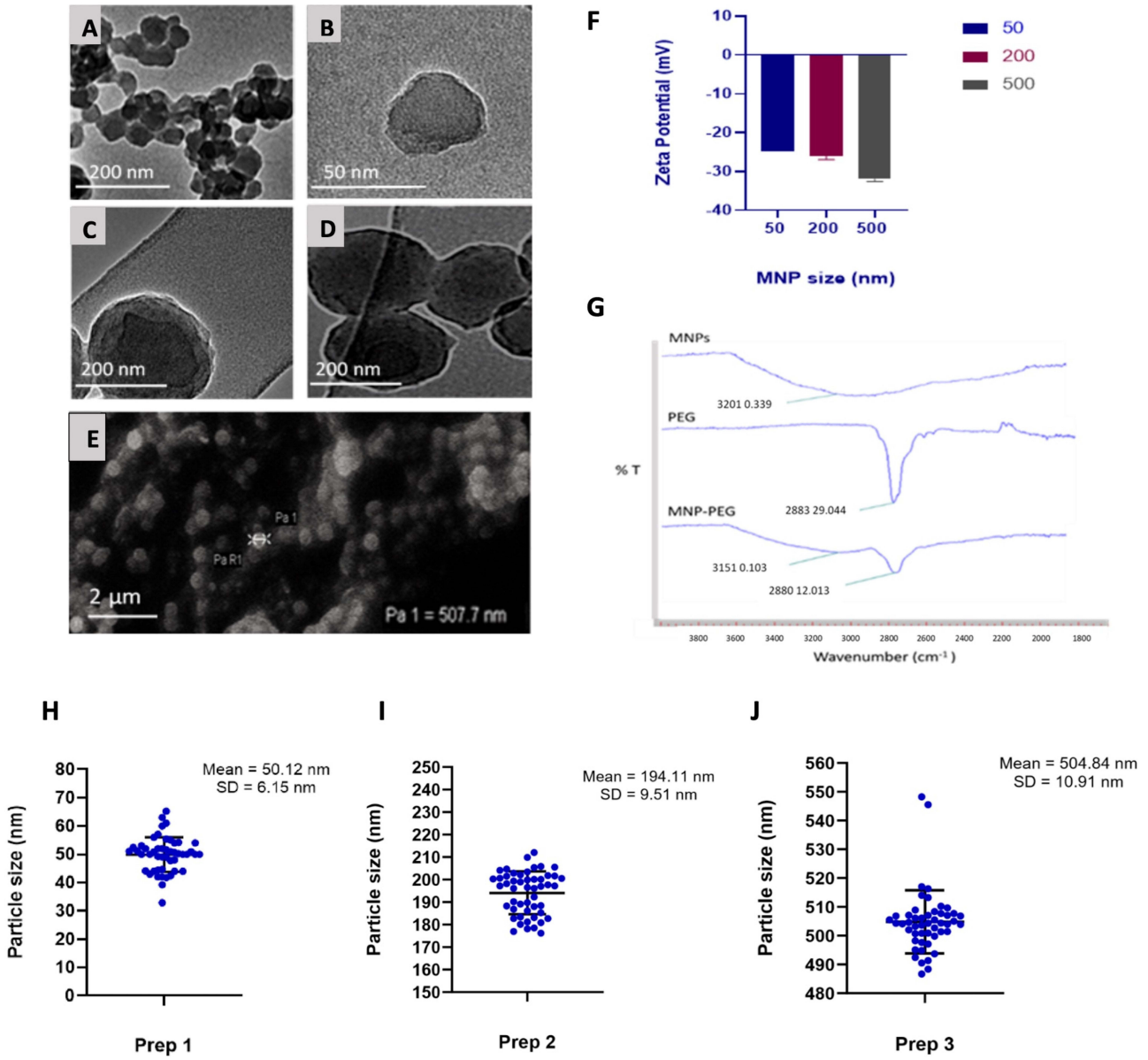

Figure 2 Characteristics of Melanin nanoparticles: TEM images of (**A** and **B**) 50 nm, (**C** and **D**) 200 nm melanin nanoparticles. (**E**) SEM image of 500 nm melanin nanoparticles. (**F**) Zeta potential of 50, 200 and 500 nm melanin nanoparticles. (**G**) FTIR to confirm melanin nanoparticles PEGylation, %T = percentage transmittance. Size distribution of melanin nanoparticles; (**H**) 50 nm (**I**) 200 nm, and (**J**) 500 nm.

was negligible on day 4 post-seeding, indicating the formation of a confluent cell layer (Figure 6A). Antibody staining for tight junction protein ZO-1 and adherent junction protein E-Cad were used to visualize the integrity of the cell barrier and cell-to-cell fusion properties on day 4 post-seeding (Figures 6B and C). Only forskolin-treated BeWo cells showed multinucleated, fused trophoblasts (Figure 6C).

Nanoparticle transfer studies were performed on day 4 post-seeding to evaluate the size dependent cut off for MNPs and MNP-PEG across the BeWo cell barrier. In parallel, positive (Antipyrine) and negative (FITC-Dextran; 40kDa) controls were run (Figure 7A and B). No difference was shown in the translocation of 50 nm MNPs across BeWo compared to the acellular control (Figure 7C). However, 200 nm MNPs were significantly retained; only 4% of the initial dose crossed the cell layer compared to 18% across the acellular control membrane (Figure 7D). Larger, 500 nm MNPs, were completely blocked by the cell barrier, but 10% of the initial dose was able to cross the acellular control membrane (Figure 7E).

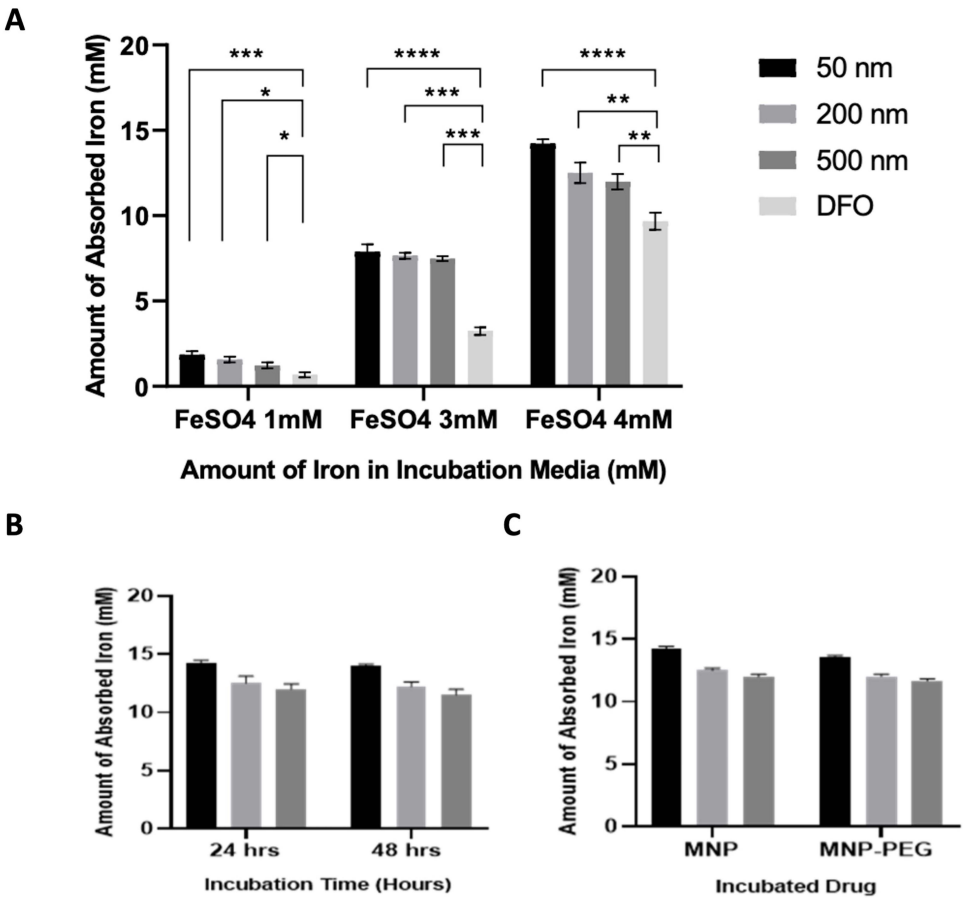

Figure 3 Efficacy of the Synthesised Nanoparticles to Chelate Iron In *Vitro*: (**A**) Graph to show a comparison of iron chelation by different sized MNPs and DFO, in iron-containing media of 1 mm to 4 mm (**B**) Graph to show a comparison of iron chelation in the 3 different diameter particles after incubation for 24 or 48 hours, (**C**) Graph to show a comparison of iron chelation in the 3 different diameter particles which are either uncoated, or surface modified with PEG. Data shows mean ± SD (n=3); *p ≤ 0.05, **p ≤ 0.01***p ≤ 0.001, ****p ≤ 0.0001.

Surface modification with PEG limited the translocation of 50 nm particles. Only 15% of the initial dose was detected in the basal chamber of the cellular insert compared to 24% in the acellular control (Figure 8A). Larger 200 nm and 500 nm PEGylated particles were completely blocked by the BeWo cell layer, but around 20% and 30% of the initial dose, respectively, were detected across the acellular membrane (Figure 8B and C). Increasing the concentration of the larger 200 and 500 nm MNP-PEG to 1 mM had no significant effect on particle translocation across the BeWo cell, whereas a significantly higher concentration (of 1 mM particles compared to the 250 μM particles) were still detected across the acellular membrane (Figure 9A and B).

Ex vivo Human Placental Perfusion

The workflow of the placental perfusion is illustrated in Figure 10. Barrier permeability was assessed by monitoring the diffusion of Antipyrine, which is known to rapidly cross the placenta and reach equal concentrations between the maternal and fetal circulation after 3 hours of perfusion (Figure 11A). Barrier integrity was confirmed by monitoring leak of perfusion of less than 3 mL/ hr (Figure 11B). Administration of 200 nm polystyrene nanoparticles, which were used as a control, shows gradual decrease of particle concentration in the maternal media and gradual increase in the fetal media. This can occur as soon as 60 minutes after the start of perfusion. However, administration of 200 nm MNP or 200 nm MNP-PEG particles were not detected in fetal circulation even after 6 hours of perfusion (Figure 11C). hCG production was not altered after the administration of nanoparticles which further confirms validity of the perfusion procedure (Figure 11D).

https://doi.org/10.2147/IJN.S494710

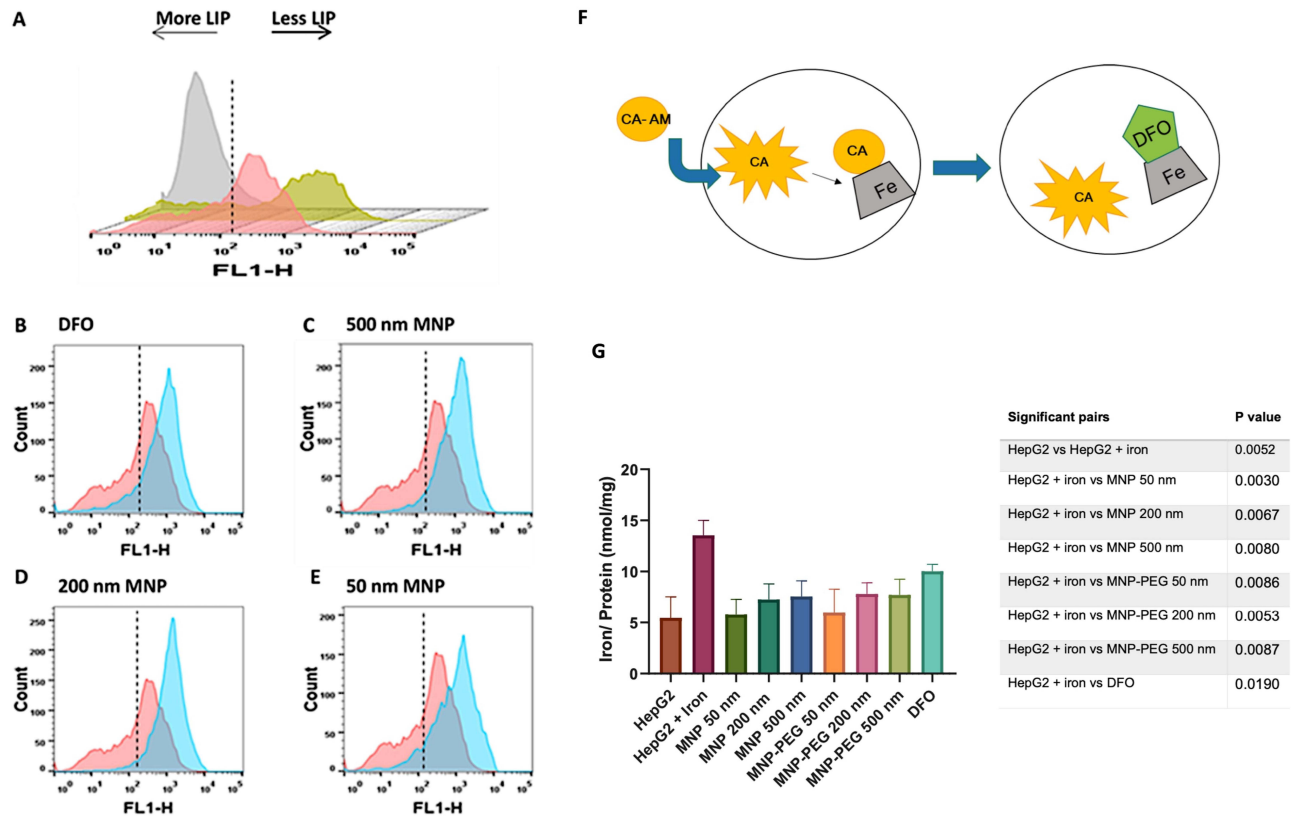

Significant pairs	P value
HepG2 vs HepG2 + iron	0.0052
HepG2 + iron vs MNP 50 nm	0.0030
HepG2 + iron vs MNP 200 nm	0.0067
HepG2 + iron vs MNP 500 nm	0.0080
HepG2 + iron vs MNP-PEG 50 nm	0.0086
HepG2 + iron vs MNP-PEG 200 nm	0.0053
HepG2 + iron vs MNP-PEG 500 nm	0.0087
HepG2 + iron vs DFO	0.0190

Figure 4 Iron chelation in HepG2 liver cells: HepG2 cells were first loaded with iron by incubating the cells with (FBS + holo transferrin) or Ferric ammonium citrate, and then stained with calcein AM. Flow cytometry analysis showing (**A**) a histogram of control unstained HepG2 cells (grey), calcein stained iron loaded HepG2 cells (pink) and calcein stained control HepG2 cells (green). Labile iron pool (LIP) in HepG2 cells before (red) and after (blue) incubation with (**B**) DFO, (**C**) 500 nm, (**D**) 200 nm and (**E**) 50 nm MNP. (**F**) A schematic diagram representing the principal of Calcein AM assay. Calcein AM hydrolysis inside the cell by intracellular esterases and gives a fluorescent signal. This signal is quenched by the intracellular LIP and reversed by adding an iron chelator. (**G**) A bar chart representing iron content in HepG2 cells (nmol per mg of protein) before and after incubating the cells with DFO and MNPs. Bars represent mean ± SD (n=3). A table represent significant pairs after multiple *t*-test (n=3).

Discussion

Improving iron chelation therapy for a safe and efficient iron overload therapy is highly desirable. Although DFO is effective in reducing iron, it has the drawback of a short half-life and requires a very long administration time (over 8–12 hrs for 5–7 days/week).[13] The ultrasmall size of nanoparticles provides a considerable number of iron binding sites due to the increased surface area, and PEGylation improves systemic circulation time. This property of the nanosized material was found to significantly reduce off target toxicity in *vivo*, where a single dose of a 1550 mg kg^{-1} nano chelator showed no evidence of tissue damage in a histological analysis of spleen, kidney and lung tissues compared to DFO which yielded in several toxicity at a much lower dose.[28] We have demonstrated in vitro that MNPs can have superior efficacy in chelating iron (up to 14 mM of iron/g of material) compared to DFO of the same concentration (Figure 3A). Surface modification with PEG did not significantly limit the ability of MNPs to adsorb iron (Figure 3C), and these two factors may lower required dosage and frequency. Similar findings were reported in an iron-overload mice models exposed to both DFO and MNP-PEG, where MNP-PEG were able to chelate a significantly higher amount of iron at one low dose (35 mg/kg) compared to 50mg/kg of DFO at five doses. Moreover, MNPs had a longer circulation half-life (17 hours compared to 5 minutes DFO in mice).[13] This significant increase in blood circulation is due to PEGylation which reduce renal and reticuloendothelial clearance, degradation, proteolysis, and immunogenicity.[29,30] Our results also showed that MNPs were able to chelate LIP in an iron loaded HepG2 cell line with higher efficacy compared to DFO (Figure 4G). Iron levels in the iron loaded HepG2 cells incubated with MNPs were returned to the normal pre-iron

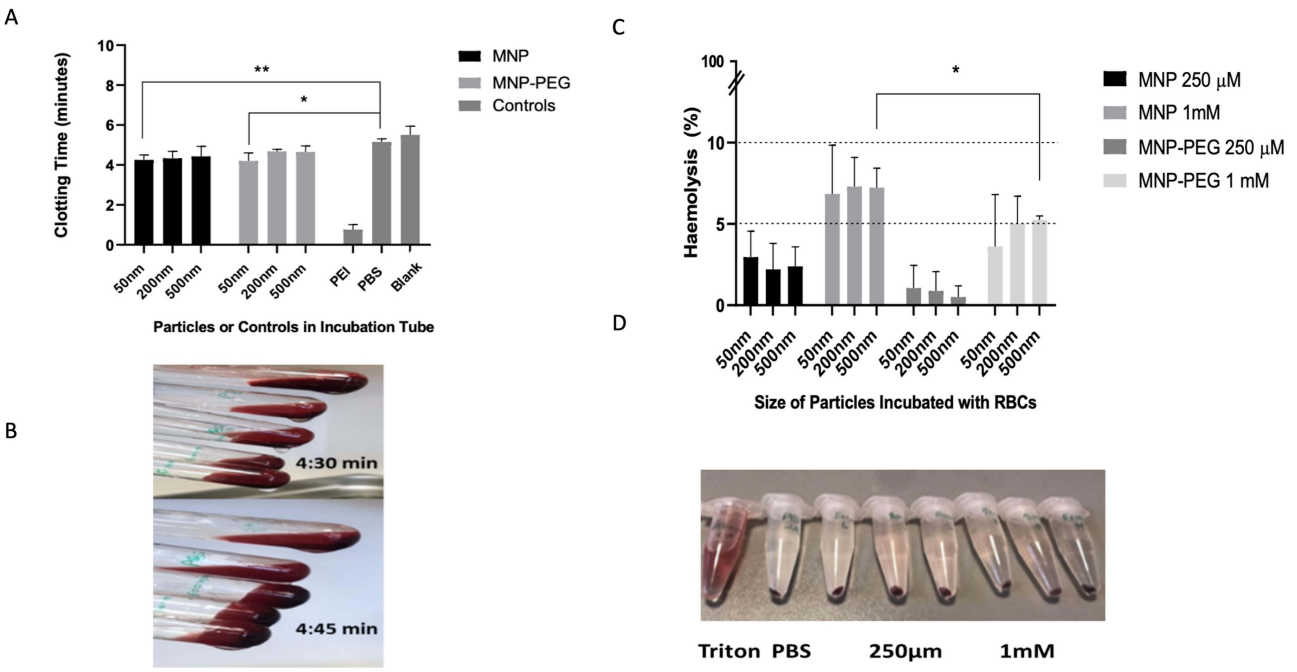

Figure 5 Compatibility in blood; coagulation and haemolysis assay: (**A**) Graph shows blood clotting time after incubation with three different sized MNPs and MNP-PEG. Polyethylenimine (PEI) was used as positive control and PBS as negative control. (**B**) Glass tubes represents clotting time of (top to bottom glass tubes) Blank, PBS, MNP sized 50, 200 and 500 nm at 4:30 min (top image) and 4:45 min (bottom images). (**C**) Graph shows percent haemolysis of RBCs induced by different sizes and concentrations of MNPs and MNP-PEG, the horizontal dashed lines represent the compatible (5%) and significant (10%) haemolysis thresholds. (**D**) Eppendorf tubes showing representative images of haemolysis induced by (left to right) the positive control Triton, the negative control PBS, 250 μM and 1mM MNP sized 50, 200 and 500 nm. Data shows mean ± SD (n=3). *p≤ 0.05; **p ≤ 0.01.

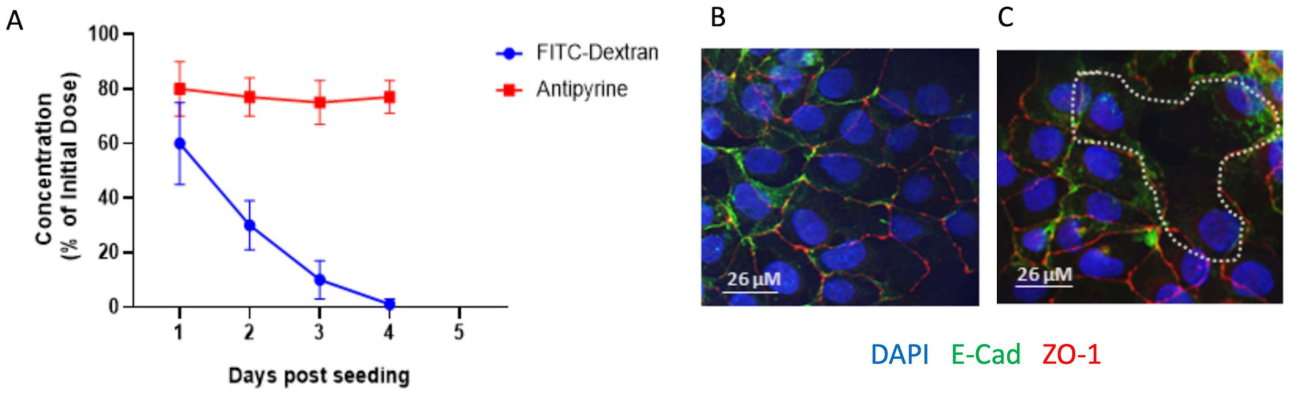

Figure 6 Confirmation of monolayer formation and BeWo syncytial fusion. (**A**) Transport of negative control FITC-Dextran (40 kDa) and positive control Antipyrine across BeWo cell layer. (**B**) Cell layers on the transwell membrane support were then imaged by confocal microscopy after staining with E-cadherin (E-Cad; green), zona occludens-1 (ZO-1; red), and DAPI (blue) treated with DMSO or (**C**) Forskolin. The dashed line represents area of cellular fusion (multinucleated) upon treatment with Forskolin which is known to enhance BeWo syncytial fusion. Data are representative of at least three different experiments. Images were acquired and analysed using Volocity software. Scale bar = 26 μm.

loading levels, suggesting that it did not reduce essential iron required for differentiation. The mechanism of MNPs reducing LIP in HepG2 is not known.

The compatibility of melanin nanoparticles with blood could mainly attribute to their biological nature and anionic charge. Many positively charged particles were found to be toxic in blood due to their interaction of the negatively charged RBCs and platelets or due to interference with the coagulation cascade.[31,32] In this study, MNPs did not generate significant haemolysis even at a high concentration (1 mM). Previous studies have demonstrated the successful intravenous administration of PEGylated MNPs in mice, highlighting their ability to circulate systemically without

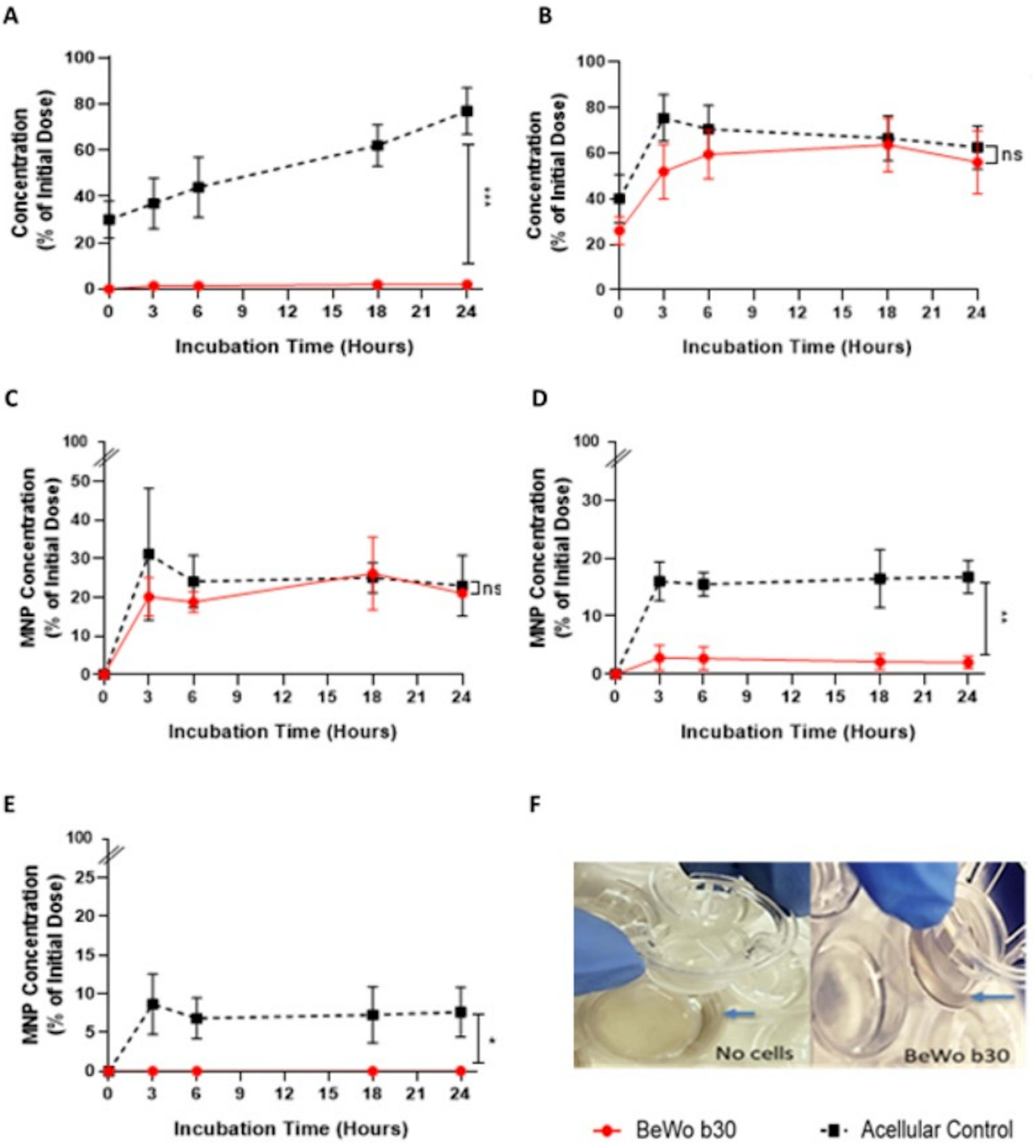

Figure 7 Comparison of passage of MNPs across BeWo cell layer or acellular control in a transwell model: Experiments were performed 4 days post-seeding (**A**) 5 μM FITCdextran 40kDa, (**B**) 100 μM antipyrine (**C**) 50 nm MNP, (**D**) 200 nm MNP and (**E**) 500 nm MNP. (**F**) Transwell insert showing comparison of MNP-PEG across BeWo and acellular control. Data shows mean ± SD (n=3 per treatment). *p≤ 0.05, **p ≤ 0.01, ***p ≤ 0.001.
Abbreviation: ns, not significant.

significant toxicity.[13,23] However, careful consideration of particle size and surface modifications is essential to avoid immune system recognition.

PEGylation of MNPs further enhances their hemocompatibility, a crucial factor for intravenous administration. PEG was first approved in the 1990s and has been shown to improve systemic circulation of drugs by reducing

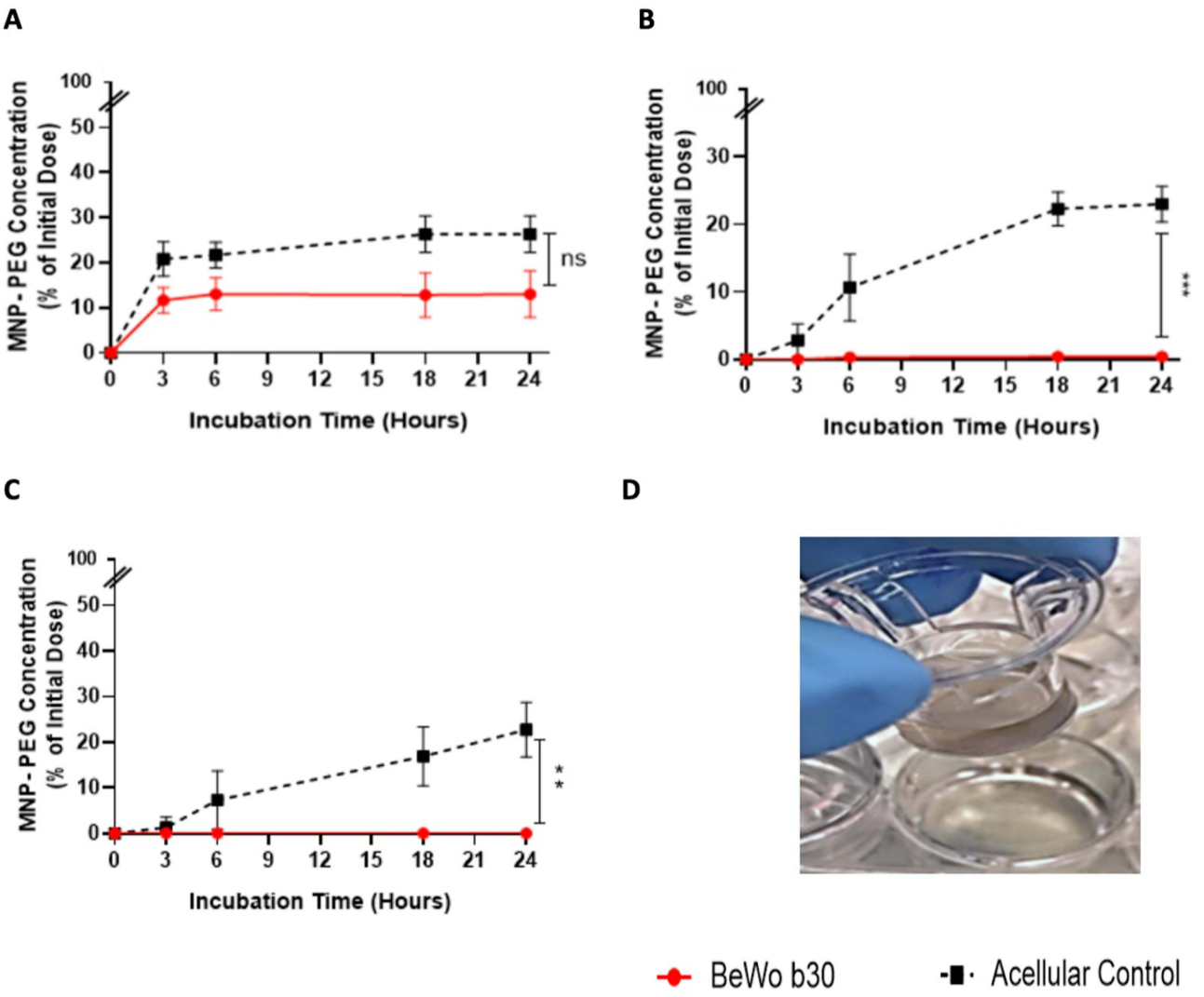

Figure 8 Comparison of passage of MNP-PEG across BeWo cell layer or acellular control in a transwell model: Transportation of MNP-PEG across BeWo monolayer and blank acellular insert on day 4 post-seeding (**A**) 50 nm, (**B**) 200 nm, and (**C**) 500 nm (n=3 per treatment). (**D**) Transwell insert of BeWo b30 of MNP-PEG in the apical chamber. Data shows mean ± SD. **p ≤ 0.01, ***p ≤ 0.001.
Abbreviation: ns, not significant.

immunogenicity and toxicity.[33,34] In our study, it was found that PEGylation of MNPs significantly improved their hemocompatibility compared to non-PEGylated particles (Figure 5A and B). This was seen in MNPs of all sizes but especially 50 nm MNPs.

Nanoparticle interaction with cells/tissue is determined by particle characteristics and functionalisation. Here it was found that interaction of MNP with choriocarcinoma cell lines and human placental perfusion is highly dependent upon particle size. When MNPs were applied into an in vitro model using human choriocarcinoma cell lines, only small particles (50 nm) were able to breach the monolayer (Figure 7C); 200 nm MNPs were partially blocked, and 500 nm MNPs did not pass at all (Figure 7D and E). This work also demonstrated that surface modification limited the transfer of the smaller MNPs and completely blocked 200 and 500 nm from passing across the cell layer in the transwell (Figure 8). A previous study using 49 and 70 nm polystyrene particles in *vitro*, reported that only 49 nm particles crossed the BeWo monolayer.[35] Surface PEGylation was also found in other studies to significantly lower placental cell and tissue uptake of liposomal doxorubicin, and it was not able to cross ex *vivo* human placenta at all.[34,36]

Previous data from a mice study using silica nanoparticles of 70 and 300 nm, showed that 70 nm particles were found in the placenta and fetal liver, but 300 nm particles did not reached the fetus.[14] Similarly, in a study involving gold

https://doi.org/10.2147/IJN.S494710

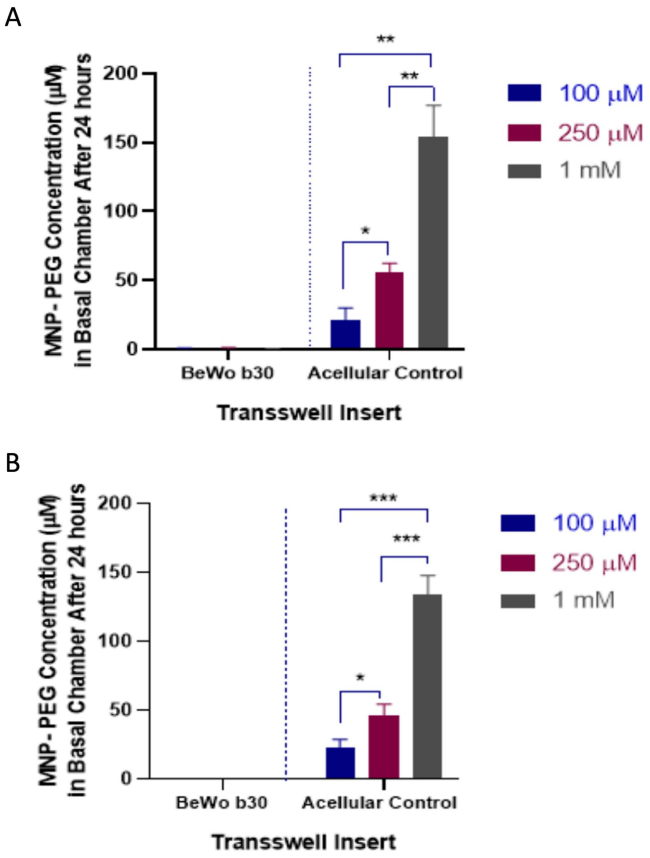

Figure 9 Effect of concentration on passage of MNP-PEG across BeWo cell layer or acellular control in a transwell model: Transport of 100 µM, 250 µM and 1 mm of (**A**) 200 nm and (**B**) 500 nm MNP-PEG across BeWo monolayer on day 4 post seeding (n=3 per treatment). Data shows mean ± SD. *p≤ 0.05; **p ≤ 0.01; ***p ≤ 0.001.

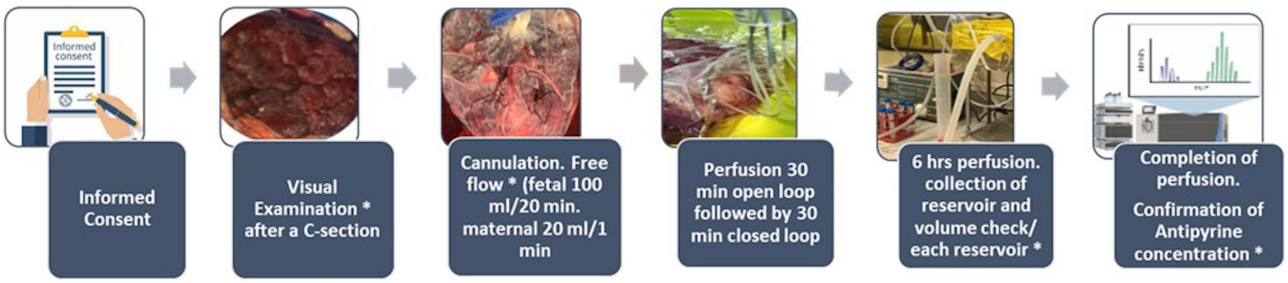

Figure 10 Workflow of human placental perfusion: Stars represent checkpoints at each step to ensure successful perfusion. Each reservoir was centrifuged at low speed to wash out cells followed by a high-speed spin to collect nanoparticles for analysis.

nanoparticles of 1.4, 18, and 80 nm through rat placenta, up to 3% of the initial dose of the smaller particles were able to cross the placenta but not the 80 nm.[16] These findings suggest that particle size plays a crucial role in placental transfer, with smaller nanoparticles more likely to cross the placental barrier. However, data from murine studies are not representative as the diffusion barrier in the murine placenta is significantly greater than human placenta.[37]

While transwell models using a BeWo cell barrier is the gold standard system in predicting transport of substances across the human placenta, it only represents the trophoblastic layer. This issue was addressed by using the ex vivo human placental perfusion system which contains the syncytiotrophoblast cell layer, connective tissue, and the fetal endothelium. The ex vivo human placental perfusion system is more representative than animal studies due to the structural differences between mice (and other animals) and human placentae. Previous results of ex vivo human placental perfusion implied that the main factor of placental uptake was particle size. In most studies, different types

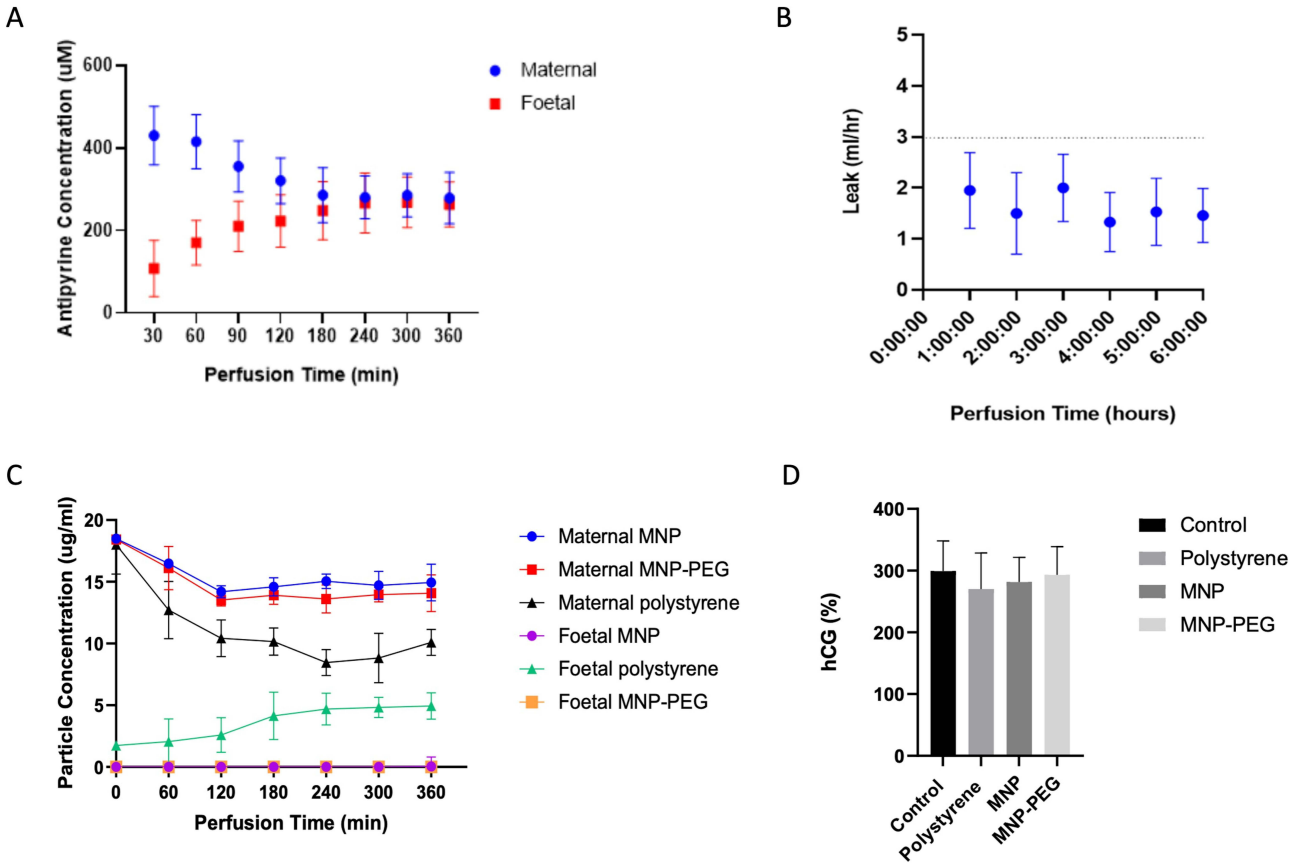

Figure 11 Transport of MNP and MNP-PEG in a perfused human placenta: (**A**) Concentration of the reference compound Antipyrine in maternal and fetal circulation of the human placental reperfusion system. (**B**) Graph shows the loss of volume before collecting reservoir at each time point throughout 6 hours perfusion. (**C**) Concentration of 200 nm MNP and MNP-PEG and polystyrene nanoparticles in maternal and fetal circulation of the perfusion system of human placenta. (**D**) Graph shows hCG production (%) after administration of polystyrene, MNP or MNP-PEG nanoparticles.

of particles larger than 80 nm did not cross the placenta.[15,18,20,22] It was suggested from the perfusion profiles that particles smaller than 80 nm crossed the barrier by diffusion. On the other hand, polystyrene nanoparticles of up to 240 nm were able to cross the placenta while the 500 nm were retained in the maternal circuit[22] indicating that other characteristics of nanoparticles such as composition or surface charge affect their interaction. When PEGylated gold particles of 3, 10, and 30 nm were applied, only 3 nm particles where able to cross the placenta.[17,18] In a different study, PEGylated gold particles of 3 nm were able to cross the placenta but carboxylated gold particles of the same size did not.[17] We found that MNP-PEG of 200 nm or above were restricted from moving across BeWo cell barrier in a transwell model, and in an ex *vivo* human placental perfusion model (Figure 11B). These findings suggest that while nanoparticle interaction with the placenta is mainly size dependent and/or due to charge/composition, it is challenging to identify the contribution of a single factor that affects this interaction.

Conclusion

This study addressed a complicated and neglected challenge during pregnancy in which a medication needs to be restricted to the maternal blood stream and not reach the fetus. Current chelation options are limited and contra-indicated. The use of melanin nanoparticles at a cut off above 200 nm could possibly provide a safer iron chelation therapy during pregnancy. However, pre-clinical studies are necessary to fully evaluate the safety of MNPs in the long-time exposure.

https://doi.org/10.2147/IJN.S494710

Acknowledgments

NB is supported by King Saud University scholarship and fellowship (KSU1659). HT would like to acknowledge the Williams Fund (Oxford Hospitals Charity #0085) for their continued support.

Funding

This research is funded by the Williams Fund (Oxford Hospitals Charity #0085) and King Saud University scholarship and fellowship (grant number KSU1659).

Disclosure

The authors report no conflicts of interest in this work.

The abstract of a small section on this paper was presented at the SMFM's 42nd Annual Pregnancy Meeting as an oral presentation with interim findings (2022, ID no.67). The abstract was published in the Supplement of the American Journal of Obstetrics & Gynecology (AJOG).

References

1. Wise J. Pregnant women should be included in clinical trials to improve outcomes, says commission. *BMJ*. 2022;377(o1193).
2. Male V. SARS-CoV-2 infection and COVID-19 vaccination in pregnancy. *Nat Rev Immunol*. 2022;22(5):277–282. doi:10.1038/s41577-022-00703-6
3. Sorrentino F, Maffei L, Caprari P, et al. Pregnancy in Thalassemia and sickle cell disease: the experience of an Italian Thalassemia Center. *Front mol Biosci*. 2020;7(16).
4. Origa R, Comitini F. Pregnancy in Thalassemia. *Mediterr J Hematol Infect Dis*. 2019;11(1):e2019019–e2019019. doi:10.4084/mjhid.2019.019
5. Vlachodimitropoulou E, Thomas A, Shah F, Kyei-Mensah A. Pregnancy and iron status in β-thalassaemia major and intermedia: six years' experience in a North London Hospital. *J Obstetrics Gynaecol*. 2018;38(4):567–570. doi:10.1080/01443615.2017.1342616
6. Thompson AA, Kim H-Y, Singer ST, et al. Pregnancy outcomes in women with thalassemia in North America and the United Kingdom. *Am J Hematol*. 2013;88(9):771–773. doi:10.1002/ajh.23506
7. Cassinerio E, Baldini IM, Alameddine RS, et al. Pregnancy in patients with thalassemia major: a cohort study and conclusions for an adequate care management approach. *Ann Hematol*. 2017;96(6):1015–1021. doi:10.1007/s00277-017-2979-9
8. Nourollahpour Shiadeh M, Cassinerio E, Modarres M, Zareiyan A, Hamzehgardeshi Z, Behboodi Moghadam Z. Reproductive health issues in female patients with beta-thalassaemia major: a narrative literature review. *J Obstetrics Gynaecol*. 2020;1–10.
9. RCOG. Management of Beta Thalassaemia in Pregnancy; Green-top Guideline No. 66. Royal college of obstetricians and gynaecologists; 2014. Available fom: https://www.rcog.org.uk/media/vz1g54xu/gtg_66_thalassaemia.pdf. Accessed April 4, 2025.
10. Nel AE, Mädler L, Velegol D, et al. Understanding biophysicochemical interactions at the nano–bio interface. *Nature Mater*. 2009;8(7):543–557. doi:10.1038/nmat2442
11. Auría-Soro C, Nesma T, Juanes-Velasco P, et al. Interactions of nanoparticles and biosystems: microenvironment of nanoparticles and biomolecules in nanomedicine. *Nanomaterials*. 2019;9(10):1365. doi:10.3390/nano9101365
12. Park J, Moon H, Hong S. Recent advances in melanin-like nanomaterials in biomedical applications: a mini review. *Biomater Res*. 2019;23(1):24. doi:10.1186/s40824-019-0175-9
13. Yan J, Ji Y, Zhang P, et al. Melanin nanoparticles as an endogenous agent for efficient iron overload therapy. *J Mater Chem B*. 2016;4(45):7233–7240. doi:10.1039/C6TB01558A
14. Yamashita K, Yoshioka Y, Higashisaka K, et al. Silica and titanium dioxide nanoparticles cause pregnancy complications in mice. *Nature Nanotechnol*. 2011;6(5):321–328. doi:10.1038/nnano.2011.41
15. Poulsen MS, Mose T, Maroun LL, Mathiesen L, Knudsen LE, Rytting E. Kinetics of silica nanoparticles in the human placenta. *Nanotoxicology*. 2015;9(Suppl 1):79–86. doi:10.3109/17435390.2013.812259
16. Semmler-Behnke M, Lipka J, Wenk A, et al. Size dependent translocation and fetal accumulation of gold nanoparticles from maternal blood in the rat. *Part Fibre Toxicol*. 2014;11:33. doi:10.1186/s12989-014-0033-9
17. Aengenheister L, Dietrich D, Sadeghpour A, et al. Gold nanoparticle distribution in advanced in vitro and ex vivo human placental barrier models. *J Nanobiotechnol*. 2018;16(1):79. doi:10.1186/s12951-018-0406-6
18. Myllynen PK, Loughran MJ, Howard CV, Sormunen R, Walsh AA, Vähäkangas KH. Kinetics of gold nanoparticles in the human placenta. *Reprod Toxicol*. 2008;26(2):130–137. doi:10.1016/j.reprotox.2008.06.008
19. Cornford EM, Hyman S, Cornford ME, et al. Non-invasive gene targeting to the fetal brain after intravenous administration and transplacental transfer of plasmid DNA using PEGylated immunoliposomes. *J Drug Targeting*. 2016;24(1):58–67. doi:10.3109/1061186X.2015.1055569
20. King A, Muller T. Using fluid-induced seismicity to infer permeability. *ASEG Extend Abstracts*. 2016;2016(1):1–5.
21. Huang J-P, Hsieh PCH, Chen C-Y, et al. Nanoparticles can cross mouse placenta and induce trophoblast apoptosis. *Placenta*. 2015;36(12):1433–1441. doi:10.1016/j.placenta.2015.10.007
22. Wick P, Malek A, Manser P, et al. Barrier capacity of human placenta for nanosized materials. *Environ Health Perspect*. 2010;118(3):432–436. doi:10.1289/ehp.0901200
23. Zhang P, Yue Y, Pan D, et al. Pharmacokinetics study of Zr-89-labeled melanin nanoparticle in iron-overload mice. *Nucl Med Biol*. 2016;43(9):529–533. doi:10.1016/j.nucmedbio.2016.05.014
24. Amin DR, Sugnaux C, Lau KHA, Messersmith PB. Size control and fluorescence labeling of polydopamine melanin-mimetic nanoparticles for intracellular imaging. *Biomimetics*. 2017;2(3):17. doi:10.3390/biomimetics2030017

25. Perring J, Crawshay-Williams F, Huang C, Townley HE. Bio-inspired melanin nanoparticles induce cancer cell death by iron adsorption. *J Mater Sci Mater Med*. 2018;29(12):181. doi:10.1007/s10856-018-6190-x
26. Eaton BM, Oakey MP. Sequential preparation of highly purified microvillous and basal syncytiotrophoblast membranes in substantial yield from a single term human placenta: inhibition of microvillous alkaline phosphatase activity by EDTA. *Biochimica Et Biophysica Acta (BBA) - Biomembranes*. 1994;1193(1):85–92. doi:10.1016/0005-2736(94)90336-0
27. Jiang Y, Li Y, Richard C, Scherman D, Liu Y. Hemocompatibility investigation and improvement of near-infrared persistent luminescent nanoparticle ZnGa2O4:Cr3+ by surface PEGylation. *J Mat Chem B*. 2019;7(24):3796–3803. doi:10.1039/C9TB00378A
28. Kang H, Han M, Xue J, et al. Renal clearable nanochelators for iron overload therapy. *Nat Commun*. 2019;10(1):5134. doi:10.1038/s41467-019-13143-z
29. Harris JM, Chess RB. Effect of pegylation on pharmaceuticals. *Nat Rev Drug Discov*. 2003;2(3):214–221. doi:10.1038/nrd1033
30. Harris JM, Martin NE, Modi M. Pegylation. *Clin Pharmacokinet*. 2001;40(7):539–551. doi:10.2165/00003088-200140070-00005
31. Guo S, Shi Y, Liang Y, Liu L, Sun K, Li Y. Relationship and improvement strategies between drug nanocarrier characteristics and hemocompatibility: what can we learn from the literature. *Asian J Pharm Sci*. 2021;16(5):551–576. doi:10.1016/j.ajps.2020.12.002
32. Svirshchevskaya EV, Zubareva AA, Boyko AA, et al. Analysis of toxicity and biocompatibility of chitosan derivatives with different physico-chemical properties. *Appl Biochem Microbiol*. 2016;52(5):483–490. doi:10.1134/S000368381605015X
33. Lammers T, Sofias AM, van der Meel R, et al. Dexamethasone nanomedicines for COVID-19. *Nature Nanotechnol*. 2020;15(8):622–624. doi:10.1038/s41565-020-0752-z
34. Parrott MC, DeSimone JM. Relieving PEGylation. *Nat Chem*. 2012;4(1):13–14. doi:10.1038/nchem.1230
35. Aengenheister L, Keevend K, Muoth C, et al. An advanced human in vitro co-culture model for translocation studies across the placental barrier. *Sci Rep*. 2018;8(1):5388. doi:10.1038/s41598-018-23410-6
36. Valero L, Alhareth K, Gil S, et al. Assessment of dually labelled PEGylated liposomes transplacental passage and placental penetration using a combination of two ex-vivo human models: the dually perfused placenta and the suspended villous explants. *Int J Pharm*. 2017;532(2):729–737. doi:10.1016/j.ijpharm.2017.07.076
37. Keelan JA. Nanoparticles versus the placenta. *Nature Nanotechnol*. 2011;6(5):263–264. doi:10.1038/nnano.2011.65